


Vibrational instabilities in multilayer graphene and graphite: Effects of strain and number of layersLuis D. Zambrano Palma ^{1,2,*} Marcos G. Menezes ^{1,†} and Rodrigo B. Capaz ^{1,3,‡}¹*Instituto de Física, Universidade Federal do Rio de Janeiro, 21941-972 Rio de Janeiro, RJ, Brazil*²*Facultad de Ingeniería Mecánica y Ciencias de la Producción, Escuela Superior Politécnica del Litoral, 090902 Guayaquil, Guayas, Ecuador*³*Brazilian Nanotechnology National Laboratory (LNNano), Brazilian Center for Research in Energy and Materials (CNPEM), 13083-970 Campinas, SP, Brazil* (Received 28 April 2022; revised 13 October 2022; accepted 26 October 2022; published 7 November 2022)

We study the rippling instabilities of multilayer graphene and graphite as a function of strain and number of layers using density-functional theory and density-functional perturbation theory calculations. We find that, for multilayer graphene, a small but finite compressive strain is needed to induce a rippling instability, signaled by the onset of imaginary frequencies near the center of the Brillouin zone. For monolayer graphene, this critical strain is zero within numerical uncertainty. Using insights from continuum elasticity theory, we fit the phonon dispersion of the ZA mode near the zone center to a function $\omega^2(q) = C_2q^2 + C_4q^4$ and determine the C_2 and C_4 coefficients as a function of strain and number of layers. In particular, the C_2 coefficient is positive for multilayers in the absence of strain and shows a linear dependence with strain. It assumes negative values for compressive strains beyond a critical value and it is responsible for the appearance of imaginary frequencies in the ZA mode. We discuss these results in light of both continuum and atomistic approaches. Critical parameters vary smoothly with the number of layers from monolayer graphene (two-dimensional) to graphite (three-dimensional).

DOI: [10.1103/PhysRevB.106.195407](https://doi.org/10.1103/PhysRevB.106.195407)**I. INTRODUCTION**

When we consider an ideal freestanding and unstrained two-dimensional (2D) material, it is important to note that the concept of a 2D material without any strain is simply an idealization. In many circumstances, 2D materials are exposed to strain, for example, caused by manipulation when they are deposited on a substrate. Therefore, studying 2D materials under strain is extremely important because it disturbs the vibrational stability of the system and it may produce effects such as long-wavelength rippling and affect macroscopic elastic properties such as the bending rigidity or linear elastic modulus.

In the particular case of monolayer graphene, the prototypical 2D material, there is a strong connection between the out-of-plane ZA branch of phonon dispersion and vibrational stability, with implications to the idea of the very existence of purely two-dimensional crystals. As a result, the ZA mode in graphene has been extensively studied. Early works [1–6] demonstrated how long-range order is destroyed by thermal fluctuations in low-dimensional systems. In this context, it is important to note that rippling disorder in a two-dimensional crystal such as graphene is obviously related to atomic displacements in the out-of-plane direction, hence the importance in studying the ZA vibrational modes. Experimentally, graphene ripples were studied both in suspended sheets

[7] as well as on top of various substrates [8], and rippling patterns were observed in all cases. Meanwhile, antiferromagnetic measurements were used to compare the behavior of graphene monolayers fabricated on top of SiO₂ and mica substrates and it was found that graphene is flat to the atomic level in the latter, suggesting that some component of the rippling is related to the contours of the underlying substrate [9]. These results suggest that it is fundamental to know the behavior of the intrinsic rippling pattern in graphene under strain, as the substrate may induce compressive or tensile strain on an adjacent graphene sheet due to a lattice mismatch.

The structural and vibrational stabilities of monolayer graphene under different types of uniaxial and biaxial strains in graphene have been analyzed theoretically. Analysis of the ZA phonon mode under biaxial tensile strain indicates that graphene does not have vibrational instabilities under this type of strain [10]. However, the situation is very different for compressive or shear strains. Graphene's ZA branch was found to be unstable with respect to pure shear strain [11,12]. In addition, studies of graphene under uniaxial compressive strain along both zigzag and armchair directions indicate phonon instabilities near the center of the Brillouin zone and predict that in highly strained graphene a phonon band gap will appear [13]. Similarly, Ref. [14] studied the effects of rippling induced by compressive strain and found that imaginary frequencies appear in a small region around the Γ point in the ZA dispersion. The detailed dispersion of the ZA mode near Γ has also been the focus of numerous studies. In Ref. [15], nonperturbative anharmonic calculations on graphene within the atomistic and continuum approaches suggested that unstrained graphene has a quadratic dispersion

*ldzambra@espol.edu.ec

†marcosgm@if.ufrj.br

‡rodrigo.capaz@lnnano.cnpem.br

in the ZA mode, which is the expected behavior for an elastic membrane [16]. On the other hand, Kumar *et al.* [17] found that a small linear term appears in the ZA mode dispersion of unstrained graphene, which differs from the expected purely quadratic model.

In comparison to monolayer graphene, very little is known about rippling instabilities and the ZA dispersion in multilayer graphene. Exploring the effects of thickness and interlayer interactions, including the transition from 2D (graphene) to three-dimensional (3D; graphite) regimes is extremely relevant in the context of instabilities of low-dimensional systems. Considering this scenario, in this work we examine the effects of biaxial tensile and compressive strains on the stability of monolayer, bilayer, and trilayer graphene and graphite. We also analyze in detail the dispersion of the ZA mode as a function of thickness and strain. We employ *ab initio* calculations based on density-functional theory (DFT) and density-functional perturbation theory (DFPT) and finally, we use insights from the theory of elasticity of membranes to explain the vibrational instabilities.

II. METHODS

Our DFT calculations are based on the pseudopotential method, as implemented in the QUANTUM ESPRESSO package [18]. We study monolayer, bilayer, and trilayer graphene with Bernal stacking and graphite. For the multilayers, a sufficiently large vacuum region is set for each simulation cell in the direction perpendicular to the sheets in order to avoid interactions with periodic images, with cell sizes that range from 10 Å in monolayer up to 20 Å in trilayer graphene. We used the local-density approximation (LDA) for the exchange-correlation functional in our calculations and, in the case of single-layer graphene, we also used the generalized gradient approximation (GGA) for comparison. These functionals do not include the important effects of van der Waals interactions, but LDA provides a reasonable description of the interlayer binding in multilayer graphene, as described in previous works [19]. Wave functions were expanded in a plane-wave basis with an energy cutoff of 70 Ry. We used a Monkhorst-Pack k -point grid of $35 \times 35 \times 1$ for the multilayers and $35 \times 35 \times 10$ for graphite to sample the Brillouin zone (BZ) [21]. A Gaussian smearing of 0.001 Ry was employed in all calculations.

Biaxial strain is implemented by varying the lattice parameter a in values that range from -5% to 5% of the equilibrium value in steps of 0.5% , thus spanning both tensile and compressive deformations. For each strain value (fixed lattice constant), the internal coordinates were relaxed via the conjugate gradient method and phonon dispersions were obtained by the DFPT method [22]. In this method, phonon frequencies are first calculated on a regular q -point grid for each system. We use $6 \times 6 \times 1$ grids for single-layer, bilayer, and trilayer graphene and a $6 \times 6 \times 2$ grid for graphite. After this step, the force-constant matrix in real space is evaluated by a Fourier transform, and phonon dispersions along high-symmetry directions are obtained by a second Fourier transform. Acoustic sum rules are enforced in order to guarantee that acoustic phonons have zero frequency at the Γ point. The simple algorithm from QUANTUM ESPRESSO is used, which directly corrects the diagonal components of the force-constant ma-

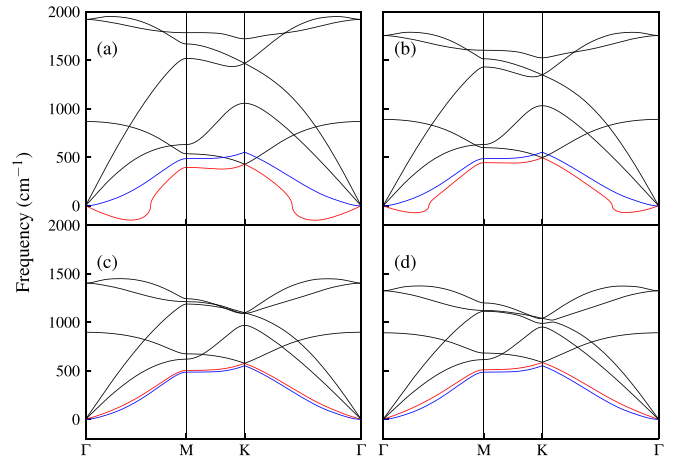


FIG. 1. Phonon dispersions for monolayer graphene in the presence of strain for (a) -5% , (b) -2.5% , (c) 2.5% , and (d) 5% . The ZA mode for each case is drawn as a red line and the same mode in the unstrained case is drawn as a blue line. Imaginary frequencies are represented as negative values.

trix. We have tested the convergence of these calculations with respect to the energy cutoff, q -grid density, and vacuum size, as described in the Supplemental Material [20]. The values reported above for these parameters are found to provide well converged values for most quantities of interest in this work. Tighter parameters are used for cases of particular interest, as we discuss below. The quality of the interpolation procedure is also discussed in the Supplemental Material.

In general, we will be particularly interested in the dispersion of the flexural ZA mode in each case. More specifically, imaginary frequencies (represented as negative values in phonon dispersion curves) that may appear in the vicinity of the Γ point correspond to structural out-of-plane instabilities that result in rippling.

III. RESULTS

A. Phonon dispersions

We begin by studying the phonon dispersions of multilayer graphene and graphite along high-symmetry paths in the BZ. From the frequency spectra we can extract useful information, such as the bending rigidity of the sheets and possible rippling instabilities. Additionally, we know that the frequencies of acoustic modes must vanish at the Γ point as a consequence of the translation symmetry and typically, in 3D systems, there is a linear relationship between the frequency ω and the modulus of the wave vector q in the vicinity of Γ . However, in the case of monolayer graphene and thin membranes in general (in equilibrium), only two of the three acoustic modes have a clearly linear dispersion, while the flexural acoustic mode (ZA mode), which is the most sensitive to mechanical stimuli such as deformations, has an apparent $\sim q^2$ dispersion. The same situation happens for graphite. We now discuss these features in detail when strain is introduced. Figures 1 and 2 show the phonon dispersions of monolayer graphene and graphite with biaxial strains of -5.0% , -2.5% , 2.5% , and 5.0% . The phonon dispersion of the ZA mode in the equilibrium situation (zero strain) is also shown for comparison (blue lines). Our

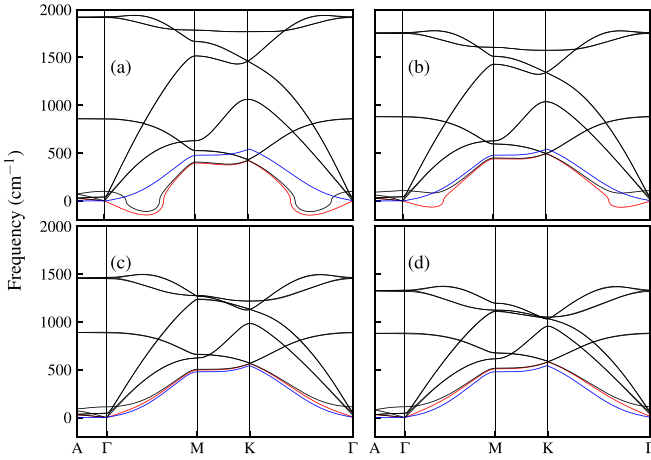


FIG. 2. Phonon dispersions for graphite in the presence of strain for (a) -5% , (b) -2.5% , (c) 2.5% , and (d) 5% . The ZA mode for each case is drawn as a red line and the same mode in the unstrained case is drawn as a blue line. Imaginary frequencies are represented as negative values.

results are in good agreement with the literature, both for the case of positive (tension) and of negative (compression) biaxial strain [10,12,13]. Note that two of the three acoustic modes follow the usual linear trend that would be expected in the vicinity of the zone center, while the ZA mode shows a very notable deviation from this behavior and it is very sensitive to the presence of strain. In particular, we notice that when single-layer graphene and graphite are subjected to a sufficiently large negative biaxial strain, imaginary frequencies appear near the center of the Brillouin zone (Γ point), which are displayed as negative values in Figs. 1 and 2. This feature indicates the presence of long-wavelength vibrational instabilities, which is a trend that is observed for negative biaxial strains in all cases studied, including bilayer and trilayer graphene, as we shall see. Previous studies demonstrate the vibrational instability of graphene under shear strain, manifested as a rippling pattern with a wavelength that decreases with the shear magnitude [12]. In a similar fashion, in our case we can see that the range of q values that result in an instability seems to increase with the magnitude of compressive strain, thus giving rise to rippling deformations with smaller wavelengths. Interestingly, the range of unstable q values seems to be roughly independent of the number of stacked layers for a given strain value, as we discuss in more detail below. A similar behavior has been found for the ZA mode of graphite, in agreement with previous works [23,24].

B. Dispersion of the ZA mode

The features described above can be understood in closer detail by analyzing the dispersion relation of the ZA phonon mode. In Fig. 3, we show the behavior of $\omega^2(q)$ in the region near the center of the Brillouin zone along the ΓM direction for single-layer graphene. The dispersion can be described as a function in which ω^2 contains both q^2 and q^4 terms in the presence of strain:

$$\omega^2 = C_2 q^2 + C_4 q^4, \quad (1)$$

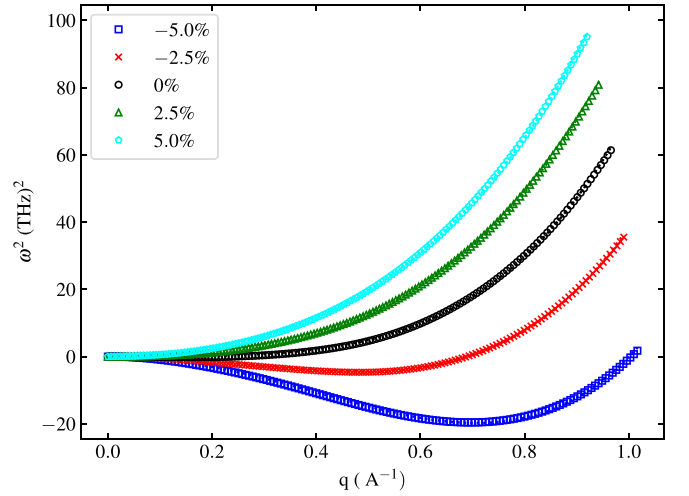


FIG. 3. Phonon dispersion of the ZA mode near the Γ point in single-layer graphene for different biaxial strain values. The lines correspond to fits of Eq. (1).

where C_2 and C_4 are constants that can be determined by fitting the squared-frequency (ω^2) vs wave-number (q) curves in Fig. 3. Equation (1) was originally applied only to tensile strains in monolayer graphene in Ref. [10], but we can see that the fit works equally well for compressive strains and multilayer systems including graphite. In fact, such a relationship is expected from the general theory of elasticity of thin membranes, where $C_4 = \kappa/\rho$ and $C_2 = 2(\lambda + \mu)\epsilon/\rho$ [25]. In these expressions, κ is the bending rigidity of the membrane, λ and μ are the Lamé coefficients, ρ is the 2D mass density, and ϵ is an applied strain. Therefore, according to elasticity theory, a purely $\omega^2 \sim q^4$ is expected in the case of a thin membrane in the absence of strain, and an additional term $C_2 q^2$ would appear only when strain is applied.

We verify this prediction by plotting the coefficients C_2 and C_4 as a function of biaxial strain for all cases studied. The results are shown in Figs. 4 and 5. In Fig. 5, we see that C_4 shows a rather weak dependence with biaxial strain, with maximum variations of about 15% with respect to the equilibrium values. On the other hand, as we see in Fig. 4, C_2 shows a stronger variation with strain. As we show in the Supplemental Material, we verify that the same behavior is observed by using a GGA functional in single-layer graphene, thus confirming the robustness of the results. As we have discussed above, according to the theory of elasticity of thin membranes, the relationship between C_2 and strain should be linear, provided that the elastic coefficients and mass density are roughly independent of strain for small deformations. Moreover, elastic theory predicts that $C_2(0) = 0$. Our results in Fig. 4 (top panel) indicate a slightly nonlinear behavior in the strain range between -5% and 5% . More importantly, the calculations indicate that $C_2(0)$ is slightly positive for multilayer systems and graphite, indicating the presence of a small q^2 term in the expression of ω^2 for zero strain, which implies a linear term in the $\omega(q)$ dispersion for small momenta. Taking this into account, we propose the following fit:

$$C_2(\epsilon) \approx C_2(0) + \alpha\epsilon + \beta\epsilon^2, \quad (2)$$

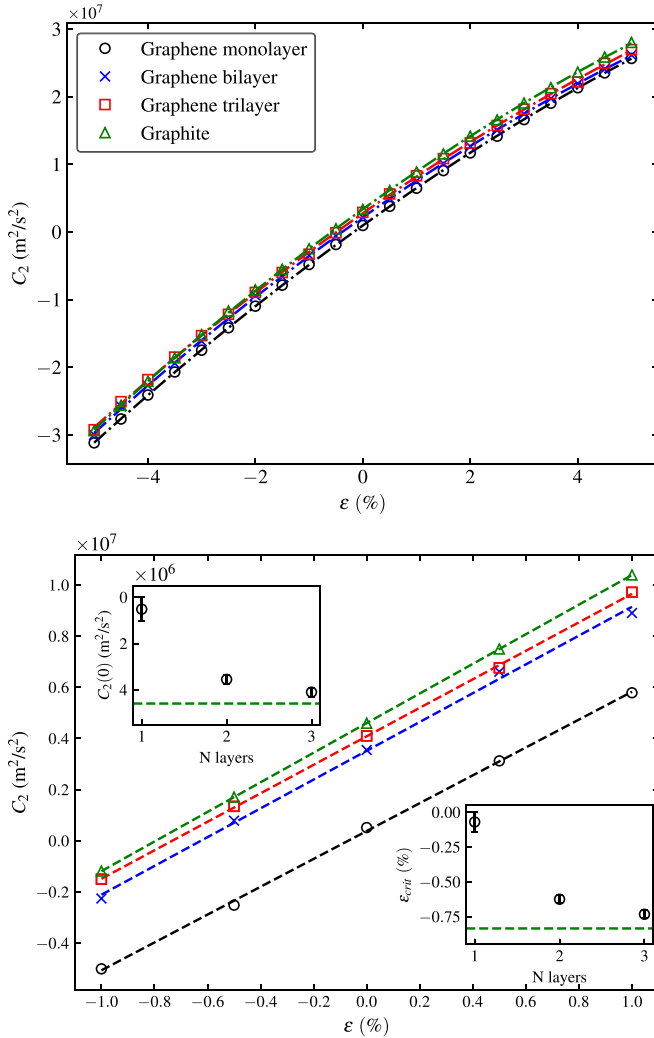


FIG. 4. Coefficient C_2 of the phonon dispersion of the ZA mode [given by fits of Eq. (1)] as a function of biaxial strain for multilayer graphene and graphite. The color coding scheme displayed in the upper panel also applies to the lower panel. The dashed lines in the C_2 upper plots correspond to fits given by Eq. (2) and the dashed lines in the C_2 lower plots correspond to fits given by Eq. (2) without the quadratic part. Tighter convergence parameters were also employed in this case (see text). Insets in the lower panel represent $C_2(0)$ (upper inset) and ϵ_{crit} (lower inset) as a function of the number of layers.

where α and β are constants and $C_2(0)$ is related to the sound velocity of the ZA mode.

The presence of a nonzero C_2 value in the ZA dispersion of unstrained graphene and 2D materials in general has been the subject of much debate for the past years. In fact, both the theory of elasticity of thin membranes and general arguments based on translation and rotational symmetries in atomistic theories state that C_2 must be zero at equilibrium [16,26–29]. In that sense, nonzero values observed in calculations should be due to numerical issues associated with the convergence parameters. On the other hand, such a nonzero value has been previously obtained by Kumar *et al.* [17] for single-layer graphene. In their calculations, a cutoff energy of 35 Ry is used, and they found that C_2 converges to a nonzero value as a function of the k -mesh density. The au-

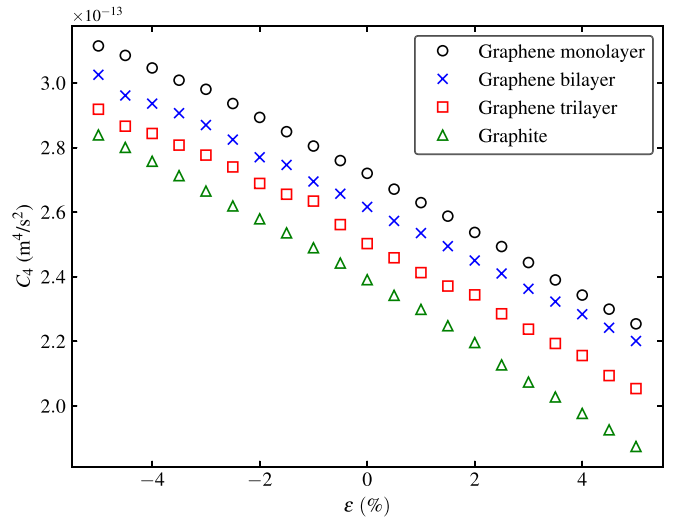


FIG. 5. Coefficients C_4 of the phonon dispersion [given by fits of Eq. (1)] as a function of biaxial strain for multilayer graphene and graphite.

thors also argue that, with a modification of the continuum Hamiltonian, justified by an analysis of atomistic restoring forces, it is possible to obtain an extra term that leads to linear dispersion and preserves rotational invariance. In addition, Ramírez *et al.* [30] found a nonzero value for $C_2(0)$ (close to $0.1/\rho$ N/m) for the same material. They employed molecular dynamics simulations with a realistic interatomic potential (LCBOPII) and concluded that the nonzero value of $C_2(0)$ affects the amplitude of out-of-plane oscillations and the crystalline membrane’s resistance to wrinkling.

In order to check this issue in detail, we have performed convergence tests for $C_2(0)$ in single-layer graphene as a function of different parameters such as the energy cutoff, vacuum size, and q -grid density. The equilibrium configuration was also carefully obtained for each set of parameters. The results are shown and discussed in detail in the Supplemental Material. The main conclusion is that $C_2(0)$ is well converged with respect to the energy cutoff and q -point grid for the set of parameters informed in the Methods section, but it has a slower convergence with respect to vacuum size. This could be related to the long-range nature of interatomic forces, which may produce spurious forces between periodic images due to out-of-plane displacements. Therefore, for a careful evaluation of this quantity, we adopt a tighter set of parameters, such as the energy cutoff (130 Ry), vacuum size (at least 30 Å), and q -point grid ($13 \times 13 \times 1$ for single-layer, bilayer, and trilayer graphene and $13 \times 13 \times 2$ for graphite), and obtain $C_2(0)$ from a fit of the $C_2(\epsilon)$ curves to Eq. (2) in the -1% to $+1\%$ region without the quadratic term, as displayed in Fig. 4 (bottom panel). The results are reported in Table I, together with the uncertainties of the fit, and can also be seen in the inset of Fig. 4 (bottom panel). As we can see, $C_2(0)$ is very close to zero in single-layer graphene, so we cannot ascertain whether it is truly nonzero within the uncertainties of the fit and the calculations. However, we can clearly see that $C_2(0)$ is nonzero for bilayer and trilayer graphene, and graphite. Its value increases with the number of

TABLE I. Coefficients C_2 at zero strain in units of m^2/s^2 [as given by the fit of Eq. (2) without the quadratic term] and critical strain $\varepsilon_{\text{crit}} \approx -C_2(0)/\alpha$.

	$C_2(0) (\times 10^7)$	$\varepsilon_{\text{crit}} (\%)$
Monolayer graphene	0.04 ± 0.04	-0.07 ± 0.07
Bilayer graphene	0.37 ± 0.02	-0.63 ± 0.03
Trilayer graphene	0.41 ± 0.02	-0.73 ± 0.03
Graphite	0.46 ± 0.02	-0.84 ± 0.02

stacked layers, showing a smooth convergence to the graphite value, suggesting that it is nonzero for multilayers in general. Such a behavior may be related to a coupling between in-plane and out-of-plane vibrations in these systems, a feature that is not found in single-layer graphene. As a consequence, a finite and negative critical strain $\varepsilon_{\text{crit}} \approx -C_2(0)/\alpha$ is needed to produce a vibrational instability in multilayer graphene sheets and its magnitude also increases with the number of layers. The values of $\varepsilon_{\text{crit}}$ are also shown in Fig. 4 (inset) and Table I.

As we mentioned above, the emergence of a linear term in the ZA dispersion of a strictly two-dimensional membrane should be prohibited because it violates rotational invariance [16,28]. Notice that this result should apply to membranes in general under zero stress. However, when an in-plane stress is applied to a graphene sheet, a nonzero torque appears under rotation, thus breaking rotational invariance. As a result, we have $C_2(\varepsilon) \neq 0$ for finite deformations and a linear term emerges in the dispersion of the ZA mode for small momenta, as we observe in our calculations.

C. Critical wave number (q_{crit})

Another important feature to analyze is the range of q values in which imaginary frequencies are observed for the ZA mode in the presence of compressive strain. These may be characterized by a critical value q_{crit} , which is the non-trivial solution of $\omega(q_{\text{crit}}) = 0$, meaning that the frequencies become real for $q > q_{\text{crit}}$. Figure 6 shows how q_{crit}^2 changes with biaxial compression and we can see that it increases with compressive strain magnitude in all cases. We can relate the value of q_{crit} to a characteristic wavelength:

$$\lambda_{\text{crit}} = \frac{2\pi}{q_{\text{crit}}} \quad (3)$$

which corresponds to the minimum wavelength of related rippling instabilities. From Eq. (1) and imposing the condition $\omega = 0$ we find $q_{\text{crit}}^2 = -C_2/C_4$. Neglecting the quadratic term in Eq. (2) and further assuming that C_4 is independent of the strain, we obtain

$$q_{\text{crit}}^2 = -\frac{\alpha}{C_4}\varepsilon - \frac{C_2(0)}{C_4}. \quad (4)$$

Following this model, we estimate that for a biaxial compression strain $\varepsilon = -2\%$, the instability region is limited up to $q_{\text{crit}} = 0.61 \text{ \AA}^{-1}$, which corresponds to a minimum wavelength $\lambda_{\text{crit}} = 11.20 \text{ \AA}$. This compares well with Ref. [14], where $\lambda_{\text{crit}} = 12 \text{ \AA}$ for the same strain magnitude is reported. Additionally, in Ref. [25], for $\varepsilon = -4\%$, $q_{\text{crit}} = 0.6 \text{ \AA}^{-1}$ is obtained, while in our work we found $q_{\text{crit}} = 0.88 \text{ \AA}^{-1}$ for the

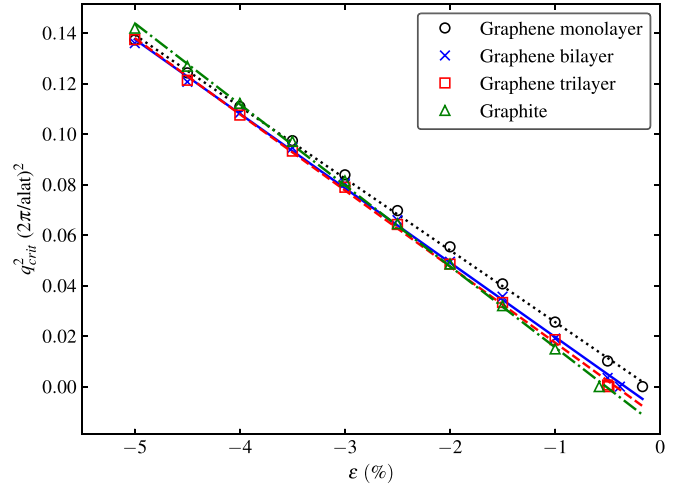


FIG. 6. Squared critical value q^2 for multilayer graphene and graphite for different values of strain. The lines correspond to the fit function shown in Eq. (4).

same strain value, again in good agreement. In Fig. 6, we see that Eq. (4) provides a good fit of the data in all cases. We also see that the influence of the layer number on the behavior of q_{crit} is quite weak.

From Eq. (4) we can obtain the minimum biaxial compressive strain needed to cause vibrational instabilities in graphene flakes of finite size l (by setting $\lambda_{\text{crit}}/2 = l$) as

$$\varepsilon_{\text{crit}} = -\frac{C_4\pi^2}{l^2} - \frac{C_2(0)}{\alpha}. \quad (5)$$

This is essentially the same dependence as the one proposed in Ref. [17], based on continuum theory for the case of uniaxial strain:

$$\varepsilon_{\text{crit}} = \frac{\left(\frac{4\pi^2}{l^2}\kappa + \mu_{\perp}\right)}{(\lambda + 2\mu)}, \quad (6)$$

where μ_{\perp} is out-of-plane shear modulus.

Finally, for all systems, we calculated mechanical properties such as the Young's modulus, third-order elastic modulus, and bending rigidity. The results are shown and discussed in detail in the Supplemental Material (see Figs. S6 and S7 and Tables S1 and S2 of the Supplemental Material [20] and see, also, Refs. [13,23,31–56] therein). For the elastic moduli, values between 1.30 and 1.32 TPa were obtained for the Young's modulus in all cases (taking into account the thicknesses of each multilayer). For the nonlinear elastic modulus, a value of $-1024.63 \text{ N m}^{-1}$ was obtained for monolayer graphene and it is roughly proportional to the number of stacked layers. These values are in good agreement with other theoretical studies and available experimental data. Finally, we find that the bending rigidity displays a near-linear dependence with the applied biaxial strain and values between 0.9 and 1.6 eV are observed in monolayer graphene. In the case of unstrained graphene, a value of about 1.31 eV was obtained, also in good agreement with other theoretical calculations. Additionally, this quantity also scales with the number of stacked layers.

IV. CONCLUSIONS

In summary, we have performed first-principles calculations based on DFPT to study the vibrational properties of multilayer graphene and graphite, with a focus on the stability of these materials to out-of-plane displacements through an analysis of the behavior of the flexural acoustic mode (ZA). Under biaxial tensile strain, no imaginary frequencies were found in the phonon dispersion, which indicates there are no long-wavelength rippling instabilities. On the other hand, for biaxial compressive strains, we see instabilities that are observed through the appearance of imaginary frequencies in the dispersion of the ZA mode near the center of the Brillouin zone.

In all cases studied, the expected quadratic dispersion for the flexural ZA frequency in equilibrium near the zone center ($\omega \simeq q^2$) must be corrected by a linear term that depends on strain. This new relationship may be described as $\omega^2 = C_2 q^2 + C_4 q^4$, where the C_2 and C_4 coefficients are obtained from a fit procedure for each value of strain. We find that, while C_4 shows a weak dependence with strain, C_2 shows a strong dependence. In particular, we find that $C_2(0)$ is nonzero for bilayer and trilayer graphene and scales with the number of stacked layers up to the limit of bulk graphite, in disagreement with predictions based on the theory of elastic membranes.

For single-layer graphene, we obtain a very small positive value for $C_2(0)$, so we cannot ascertain whether it is zero or not within the uncertainties of the fit procedure and the calculations. In all cases, for sufficiently large negative strains (below the critical value $\varepsilon_{\text{crit}}$), C_2 assumes negative values, so it is responsible for the emergence of imaginary frequencies and rippling instabilities. This behavior is observed regardless of the number of stacked layers.

We have also studied the range of q values in the BZ for which the instability is observed. This may be described by a critical value q_{crit} , which is related to the minimum wavelength of the associated out-of-plane deformations. We observe that for each value of strain the instability region has roughly the same size, regardless of the number of stacked layers. Additionally, q_{crit}^2 shows a linear dependence with strain, in agreement with the phonon dispersion and the behavior of C_2 .

ACKNOWLEDGMENTS

We thank CNPq, CAPES, FAPERJ, FAPESP, and INCT Carbon Nanomaterials for financial support. We also thank LNCC-MCTI and NACAD-UFRJ for the computational resources employed in this work.

-
- [1] R. Peierls, Quelques propriétés typiques des corps solides, *Ann. Inst. Henri Poincaré* **5**, 177 (1935).
 - [2] R. Peierls, Bemerkungen über umwandlungstemperaturen, *Helv. Phys. Acta* **7**, 81 (1934).
 - [3] L. D. Landau, On the theory of phase transitions, *Phys. Z. Sowjetunion* **11**, 26 (1937).
 - [4] E. M. Lifshitz and L. D. Landau, *Statistical Physics: Theory of the Condensed State*, Part 2 (Course of Theoretical Physics) (Butterworth-Heinemann, Washington, DC, 1980), Vol. 9.
 - [5] N. D. Mermin and H. Wagner, Absence of Ferromagnetism or Antiferromagnetism in One- or Two-Dimensional Isotropic Heisenberg Models, *Phys. Rev. Lett.* **17**, 1133 (1966).
 - [6] N. D. Mermin, Crystalline order in two dimensions, *Phys. Rev.* **176**, 250 (1968).
 - [7] J. C. Meyer, A. K. Geim, M. I. Katsnelson, K. S. Novoselov, T. J. Booth, and S. Roth, The structure of suspended graphene sheets, *Nature (London)* **446**, 60 (2007).
 - [8] U. Stöberl, U. Wurstbauer, W. Wegscheider, D. Weiss, and J. Eroms, Morphology and flexibility of graphene and few-layer graphene on various substrates, *Appl. Phys. Lett.* **93**, 051906 (2008).
 - [9] C. H. Lui, L. Liu, K. F. Mak, G. W. Flynn, and T. F. Heinz, Ultraflat graphene, *Nature (London)* **462**, 339 (2009).
 - [10] B. Rakshit and P. Mahadevan, Absence of rippling in graphene under biaxial tensile strain, *Phys. Rev. B* **82**, 153407 (2010).
 - [11] S. V. Dmitriev, Y. A. Baimova, A. Savin, and Y. S. Kivshar, Stability range for a flat graphene sheet subjected to in-plane deformation, *JETP Lett.* **93**, 571 (2011).
 - [12] G. Cocco and V. Fiorentini, Vibrational stability of graphene under combined shear and axial strains, *Phys. Rev. B* **92**, 045411 (2015).
 - [13] F. Liu, P. Ming, and J. Li, *Ab initio* calculation of ideal strength and phonon instability of graphene under tension, *Phys. Rev. B* **76**, 064120 (2007).
 - [14] P. L. de Andres, F. Guinea, and M. I. Katsnelson, Density functional theory analysis of flexural modes, elastic constants, and corrugations in strained graphene, *Phys. Rev. B* **86**, 245409 (2012).
 - [15] U. Aseginolaza, T. Cea, R. Bianco, L. Monacelli, M. Calandra, A. Bergara, F. Mauri, and I. Errea, Bending rigidity and sound propagation in graphene, [arXiv:2005.12047](https://arxiv.org/abs/2005.12047).
 - [16] M. I. Katsnelson, *Graphene: Carbon in Two Dimensions* (Cambridge University Press, Cambridge, UK, 2012).
 - [17] S. Kumar, K. P. S. S. Hembram, and U. V. Waghmare, Intrinsic buckling strength of graphene: First-principles density functional theory calculations, *Phys. Rev. B* **82**, 115411 (2010).
 - [18] P. Giannozzi, S. Baroni, N. Bonini, M. Calandra, R. Car, C. Cavazzoni, D. Ceresoli, G. L. Chiarotti, M. Cococcioni, I. Dabo *et al.*, QUANTUM ESPRESSO: a modular and open-source software project for quantum simulations of materials, *J. Phys.: Condens. Matter* **21**, 395502 (2009).
 - [19] R. R. Del Grande, M. G. Menezes, and R. B. Capaz, Layer breathing and shear modes in multilayer graphene: a DFT-vdW study, *J. Phys.: Condens. Matter* **31**, 295301 (2019).
 - [20] See Supplemental Material at <http://link.aps.org/supplemental/10.1103/PhysRevB.106.195407> for an analysis and further plots of behavior of mechanical properties as a function of biaxial strain in each of the studied cases.
 - [21] H. J. Monkhorst and J. D. Pack, Special points for Brillouin-zone integrations, *Phys. Rev. B* **13**, 5188 (1976).

- [22] S. Baroni, S. De Gironcoli, A. Dal Corso, and P. Giannozzi, Phonons and related crystal properties from density-functional perturbation theory, *Rev. Mod. Phys.* **73**, 515 (2001).
- [23] L. Karssemeijer and A. Fasolino, Phonons of graphene and graphitic materials derived from the empirical potential LCBOPII, *Surf. Sci.* **605**, 1611 (2011).
- [24] G. Kresse, J. Furthmüller, and J. Hafner, *Ab initio* force constant approach to phonon dispersion relations of diamond and graphite, *Europhys. Lett.* **32**, 729 (1995).
- [25] P. L. de Andres, F. Guinea, and M. I. Katsnelson, Bending modes, anharmonic effects, and thermal expansion coefficient in single-layer and multilayer graphene, *Phys. Rev. B* **86**, 144103 (2012).
- [26] I. M. Lifshitz, Thermal properties of chain and layered structures at low temperatures, *Zh. Eksp. Teor. Fiz.* **22**, 475 (1952).
- [27] A. Croy, Bending rigidities and universality of flexural modes in 2D crystals, *JPhys. Mater.* **3**, 02LT03 (2020).
- [28] E. Mariani and F. von Oppen, Flexural Phonons in Free-Standing Graphene, *Phys. Rev. Lett.* **100**, 076801 (2008).
- [29] M. I. Katsnelson and A. Fasolino, Graphene as a prototype crystalline membrane, *Acc. Chem. Res.* **46**, 97 (2013).
- [30] R. Ramírez and C. P. Herrero, Elastic properties and mechanical tension of graphene, *Phys. Rev. B* **95**, 045423 (2017).
- [31] J. P. Perdew, K. Burke, and M. Ernzerhof, Generalized Gradient Approximation Made Simple, *Phys. Rev. Lett.* **77**, 3865 (1996).
- [32] J. P. Perdew and A. Zunger, Self-interaction correction to density-functional approximations for many-electron systems, *Phys. Rev. B* **23**, 5048 (1981).
- [33] C. Lee, X. Wei, J. W. Kysar, and J. Hone, Measurement of the elastic properties and intrinsic strength of monolayer graphene, *Science* **321**, 385 (2008).
- [34] X. Wei, B. Fragneaud, C. A. Marianetti, and J. W. Kysar, Nonlinear elastic behavior of graphene: *Ab initio* calculations to continuum description, *Phys. Rev. B* **80**, 205407 (2009).
- [35] E. Cadelano, P. L. Palla, S. Giordano, and L. Colombo, Nonlinear Elasticity of Monolayer Graphene, *Phys. Rev. Lett.* **102**, 235502 (2009).
- [36] O. Blakslee, D. Proctor, E. Seldin, G. Spence, and T. Weng, Elastic constants of compression-annealed pyrolytic graphite, *J. Appl. Phys.* **41**, 3373 (1970).
- [37] Q. He, Y.-H. Chu, J. T. Heron, S. Y. Yang, W. I. Liang, C. Y. Kuo, H. J. Lin, P. Yu, C. W. Liang, R. J. Zeches, W. C. Kuo, J. Y. Juang, C. T. Chen, E. Arenholz, A. Scholl, and R. Ramesh, Electrically controllable spontaneous magnetism in nanoscale mixed phase multiferroics, *Nat. Commun.* **2**, 225 (2011).
- [38] G. Van Lier, C. Van Alsenoy, V. Van Doren, and P. Geerlings, *Ab initio* study of the elastic properties of single-walled carbon nanotubes and graphene, *Chem. Phys. Lett.* **326**, 181 (2000).
- [39] E. Konstantinova, S. O. Dantas, and P. M. V. B. Barone, Electronic and elastic properties of two-dimensional carbon planes, *Phys. Rev. B* **74**, 035417 (2006).
- [40] K. N. Kudin, G. E. Scuseria, and B. I. Yakobson, C₂F, BN, and C nanoshell elasticity from *ab initio* computations, *Phys. Rev. B* **64**, 235406 (2001).
- [41] D. Sánchez-Portal, E. Artacho, J. M. Soler, A. Rubio, and P. Ordejón, *Ab initio* structural, elastic, and vibrational properties of carbon nanotubes, *Phys. Rev. B* **59**, 12678 (1999).
- [42] B. Hajgato, S. Guryel, Y. Dauphin, J.-M. Blairon, H. E. Miltner, G. Van Lier, F. De Proft, and P. Geerlings, Theoretical investigation of the intrinsic mechanical properties of single- and double-layer graphene, *J. Phys. Chem. C* **116**, 22608 (2012).
- [43] E. Hernandez, C. Goze, P. Bernier, and A. Rubio, Elastic Properties of C and B_xC_yN_z Composite Nanotubes, *Phys. Rev. Lett.* **80**, 4502 (1998).
- [44] H. Zhao, K. Min, and N. R. Aluru, Size and chirality dependent elastic properties of graphene nanoribbons under uniaxial tension, *Nano Lett.* **9**, 3012 (2009).
- [45] S. Gupta, K. Dharamvir, and V. K. Jindal, Elastic moduli of single-walled carbon nanotubes and their ropes, *Phys. Rev. B* **72**, 165428 (2005).
- [46] B. WenXing, Z. ChangChun, and C. WanZhao, Simulation of Young's modulus of single-walled carbon nanotubes by molecular dynamics, *Phys. B: Condens. Matter* **352**, 156 (2004).
- [47] M. Meo and M. Rossi, Prediction of Young's modulus of single wall carbon nanotubes by molecular-mechanics based finite element modelling, *Compos. Sci. Technol.* **66**, 1597 (2006).
- [48] T. Chang and H. Gao, Size-dependent elastic properties of a single-walled carbon nanotube via a molecular mechanics model, *J. Mech. Phys. Solids* **51**, 1059 (2003).
- [49] Y. Wei, B. Wang, J. Wu, R. Yang, and M. L. Dunn, Bending rigidity and Gaussian bending stiffness of single-layered graphene, *Nano Lett.* **13**, 26 (2013).
- [50] Q. Lu, M. Arroyo, and R. Huang, Elastic bending modulus of monolayer graphene, *J. Phys. D* **42**, 102002 (2009).
- [51] N. Lindahl, D. Midtvedt, J. Svensson, O. A. Nerushev, N. Lindvall, A. Isacson, and E. E. Campbell, Determination of the bending rigidity of graphene via electrostatic actuation of buckled membranes, *Nano Lett.* **12**, 3526 (2012).
- [52] R. Nicklow, N. Wakabayashi, and H. Smith, Lattice dynamics of pyrolytic graphite, *Phys. Rev. B* **5**, 4951 (1972).
- [53] P. Koskinen and O. O. Kit, Approximate modeling of spherical membranes, *Phys. Rev. B* **82**, 235420 (2010).
- [54] J. Tersoff, Energies of fullerenes, *Phys. Rev. B* **46**, 15546 (1992).
- [55] Z.-C. Tu and Zhong-can Ou-Yang, Single-walled and multiwalled carbon nanotubes viewed as elastic tubes with the effective Young's moduli dependent on layer number, *Phys. Rev. B* **65**, 233407 (2002).
- [56] M. Arroyo and T. Belytschko, Finite crystal elasticity of carbon nanotubes based on the exponential Cauchy-Born rule, *Phys. Rev. B* **69**, 115415 (2004).